

Near-Real-Time Conflict-Related Fire Detection Using Unsupervised Deep Learning and Satellite Imagery

Kuldip Singh Atwal^{1,*}, Dieter Pfoser¹, Daniel Rothbart²

¹*Geography and Geoinformation Science, George Mason University, 4400 University Drive, Fairfax, 22030, VA, United States*

²*The Jimmy and Rosalynn Carter School for Peace and Conflict Resolution, George Mason University, 4400 University Drive, Fairfax, 22030, VA, United States*

Abstract

Ongoing armed conflict in Sudan highlights the need for rapid monitoring of conflict-related fire damage. Recent advances in deep learning and high-frequency satellite imagery enable near-real-time assessment of active fires and burn scars in war zones. This study presents a near-real-time monitoring approach using a lightweight Variational Auto-Encoder (VAE)-based model integrated with 4-band Planet Labs imagery at 3 m spatial resolution. We demonstrate that conflict-related fire damage can be detected with minimal delay using accessible, commercially available satellite data. To achieve this, we adapt a VAE-based model, originally designed for 10-band imagery, to operate effectively on high-resolution 4-band inputs. The model is trained in a unsupervised manner to learn compact latent representations of nominal land-surface conditions and identify fire-affected areas by quantifying changes between temporally paired latent embeddings. Performance is evaluated across five case studies in Sudan and compared against a cosine-distance baseline computed between temporally paired image tiles using precision, recall, F1-score, and the area under the precision-recall curve (AUPRC). Results show that the proposed approach consistently outperforms the baseline, achieving higher recall and F1-scores while maintaining strong precision in highly imbalanced fire-detection scenarios. Experiments with 8-band imagery and temporal image sequences yield only marginal per-

*Corresponding author

Email addresses: katwal@gmu.edu (Kuldip Singh Atwal), dpfoser@gmu.edu (Dieter Pfoser), drothbar@gmu.edu (Daniel Rothbart)

formance gains over single 4-band inputs, underscoring the effectiveness of the proposed lightweight approach for scalable, near-real-time conflict monitoring.

Keywords:

Conflict-related fire monitoring, Unsupervised deep learning, Variational autoencoder (VAE), Latent-space change detection, High-resolution satellite imagery, Near-Real-Time monitoring, Fire damage detection, Conflict Monitoring

1. Introduction

An armed conflict in Sudan, which began in April 2023, has resulted in widespread civilian harm, large-scale displacement, and severe destruction of infrastructure. Fighting between the Sudanese Armed Forces (SAF) and the Rapid Support Forces (RSF) has resulted in the deaths of thousands of people and the displacement of over 12 million individuals (Birch et al., 2024). The conflict initially concentrated in Khartoum state before expanding to western and southern regions, particularly Darfur, where attacks on civilians, healthcare facilities, and essential infrastructure are extensively documented (Milton et al., 2025; Dahab et al., 2025). (Eljack et al., 2023) and (Alrawa et al., 2023) highlight the impact of conflict on health.

The Sudan Conflict Observatory (SCO) has reported a massacre of more than a thousand civilians by June 2023 in El-Geneina (Rothbart et al., 2025), and reported destruction of healthcare facilities (Abubakr et al., 2024). Figure 1 shows the map of attacks in Sudan. The timeline indicates a rising number of attacks since April 2023, with a significant increase in the regions of Khartoum, El Fasher, and El Geneina.

1.1. Problem Statement and Objectives

Monitoring conflict-related fires in active war zones presents several challenges. Ground-based reporting is often delayed, incomplete, or impossible due to insecurity and access constraints (Sticher et al., 2023). As a result, satellite imagery has become a critical source of independent evidence for tracking attacks, infrastructure destruction, and potential violations of international humanitarian law (Hassan and Ahmed, 2025). Among observable conflict evidence, active fires and burn scars are particularly informative, as they frequently accompany airstrikes, shelling, looting, and the destruction of

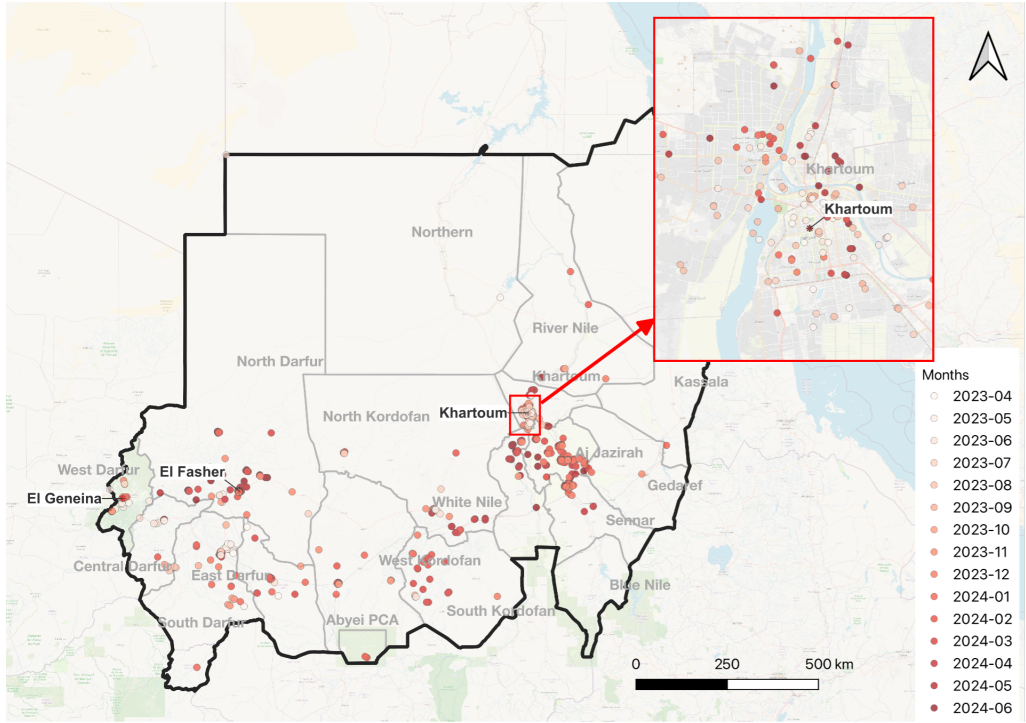


Figure 1: Map of attacks in Sudan, April–June 2023, highlighting the key conflict hotspots.

civilian structures. Recent advances in high-resolution, high-frequency satellite imagery, combined with deep learning techniques, enable the possibility of near-real-time conflict monitoring. Commercial satellite constellations, such as Planet Labs, provide near-daily revisit capabilities at meter-scale resolution, which makes them particularly suitable for detecting small-scale fires in dense environments. Similarly, deep learning methods provide a way to detect anomalous events without relying on ground-truth labels, which are limited in active conflict zones (Aung et al., 2021). However, existing fire-detection and damage-assessment methods face key limitations in conflict settings. Many approaches rely on coarse-resolution sensors, supervised learning pipelines, or computationally intensive models that are not easily scalable for rapid deployment (Racek et al., 2025). Moreover, models trained on wildfire datasets often perform poorly in urban conflict zones, where fires are short-lived, spatially fragmented (Mueller et al., 2021; Di Martino et al., 2023), and embedded in heterogeneous landscapes (Pleniou and Koutsias, 2025; Franquesa et al., 2022). These constraints hinder timely detection of

fire-affected areas, which is critical for humanitarian assessment and operational decision-making.

This study addresses these challenges by leveraging high-frequency, high-resolution PlanetScope imagery within a lightweight, unsupervised deep learning framework. The proposed approach enables scalable, near-real-time monitoring in resource-constrained environments, without relying on ground-truth labels or computationally intensive processing pipelines. The following research questions guide this work:

- Can conflict-related fire-affected areas be reliably detected in near-real time using high-frequency, high-resolution commercial satellite imagery?
- How effectively can a lightweight, unsupervised deep learning framework identify fire-affected regions compared to a traditional pixel-wise baseline?
- What is the marginal utility of short temporal sequences and additional spectral bands compared to single-snapshot multispectral imagery?

The scope of this study is limited to satellite-based observations in Sudan and focuses on the detection of fires and burn scars. Retrospective damage assessment and causal attribution are beyond the scope of this work. The framework is designed for near-real-time monitoring, prioritizing the recall of fire-affected areas while maintaining operationally viable precision. We assume the availability of cloud-free imagery or the application of standard cloud-masking techniques, recognizing that dense cloud cover remains a limitation of optical remote sensing.

The specific objectives of this study are to:

- Adapt a Variational Autoencoder (VAE)-based architecture for 3 m-resolution PlanetScope imagery using four spectral bands.
- Benchmark the framework against pixel-wise baselines using quantitative performance metrics.
- Assess the impact of additional temporal and spectral information on detection performance.

Collectively, these contributions provide an operationally viable, unsupervised approach for near-real-time detection of conflict-related fire-affected areas. Furthermore, the study empirically quantifies the marginal benefits of short temporal sequences and additional spectral bands for improving detection performance in conflict settings.

2. Related Work

2.1. Deep Learning in Fire Detection

Convolutional Neural Networks (CNNs) are widely adopted for automating fire detection from satellite imagery by identifying thermal anomalies or spectral signatures of burn scars (Toan et al., 2019; Seydi et al., 2022). Architectures like U-Net improve pixel-wise segmentation, enabling finer distinctions between active fires and background vegetation (Hally et al., 2019). More recently, Vision Transformers (ViTs) have demonstrated improved performance in capturing long-range spatial dependencies compared to traditional CNNs (Saleh et al., 2024). However, these supervised models remain heavily dependent on high-quality, labeled training data, which is scarce in active conflict zones. Moreover, while medium-resolution sensors like Moderate Resolution Imaging Spectroradiometer (MODIS) and Visible Infrared Imaging Radiometer Suite (VIIRS) are effective at thermal sensing, they often struggle to capture small-scale fires in dense or irregular settlements (Bromley, 2010; Zhao et al., 2023).

2.2. Challenges in Conflict Monitoring and Damage Assessment

Automated satellite-based conflict monitoring has advanced substantially, yet manual interpretation remains prevalent for assessing conflict-related damage (Avtar et al., 2021). Early studies relied on handcrafted features derived from Very High Resolution (VHR) imagery for post-conflict damage assessment, such as in the Gaza Strip (Kahraman et al., 2016). Subsequent studies applied supervised and semi-supervised learning approaches to detect damaged infrastructure in Syria using VHR imagery (Lee et al., 2020; Mueller et al., 2021). While effective, these methods depend on expensive imagery, labeled training data, and retrospective pre- and post-event comparisons, limiting their scalability and timeliness over large geographic extents. Research in Sudan and Darfur has historically utilized MODIS data, which, despite its efficacy in detecting large-scale events, struggles to identify the smaller, dispersed fires typical of irregular warfare (Bromley, 2010; Cornebise et al.,

2018). Time-series and change detection methods have also been explored in conflict contexts (Jenerowicz et al., 2010; Braun, 2018). However, these approaches typically focus on post-conflict or long-term damage assessment rather than near-real-time fire detection, highlighting the need for scalable, unsupervised methods capable of rapid detection, as proposed in this study. Case studies across conflict and disaster settings, including Myanmar (Marx et al., 2019) and Turkey (Kurnaz et al., 2020), demonstrate the potential of satellite imagery for fire detection, yet a gap remains in fully unsupervised methods capable of processing high-resolution data streams without labels (Xu et al., 2022).

2.3. Unsupervised Learning and Anomaly Detection

To mitigate label dependency, recent work has increasingly explored unsupervised anomaly detection, in which models learn the distribution of nominal land cover and identify deviations without requiring explicit annotations (An and Cho, 2015). Variational Autoencoders (VAEs) are frequently employed in this setting due to their ability to learn compact latent representations of complex imagery (Kingma et al., 2013). While many approaches rely on reconstruction error as an anomaly signal, prior studies have shown that reconstruction-based scores can be unreliable in fully unsupervised settings, particularly for high-capacity models (Merrill and Eskandarian, 2020). More recent work has therefore emphasized the use of latent representations for comparing imagery across time, framing anomaly detection as a form of change detection in latent space (Bergamasco et al., 2022). This approach is particularly relevant in conflict zones, where unprecedented events and limited historical labels make representation-based change detection more robust than reconstruction-based anomaly scoring.

2.4. Sensor Selection and Data Processing

Satellite sensor choice determines the trade-off between spatial resolution and temporal frequency. Landsat and Sentinel-2 provide valuable multispectral data for burn scar analysis; however, their revisit intervals of 5–10 days often miss short-lived fire events (Schroeder et al., 2016). Synthetic Aperture Radar (SAR) can penetrate cloud cover to assess post-fire land changes, though it lacks the spectral signatures provided by optical sensors (Narvaez Luces et al., 2023). PlanetScope imagery offers a balance, providing 3 m resolution and near-daily revisit cadences. However, leveraging this data for conflict monitoring requires robust preprocessing and computationally

efficient models capable of handling large daily data volumes, factors that have limited its adoption in fully unsupervised, near-real-time fire detection workflows (Boroujeni et al., 2024; de Almeida Pereira et al., 2021; Bazi et al., 2021).

3. Study area

This study focuses on five conflict-related fire incidents in the El Fasher and Khartoum regions of Sudan. In Khartoum State, an airstrike reportedly carried out by the Sudanese Armed Forces (SAF) on May 25, 2024, targeted the Gandahar Market in Omdurman. The Conflict Observatory documented damage to at least 31 structures resulting from this incident (Etefa, 2026). PlanetScope imagery acquired on the day of the strike shows a visible smoke plume over the market area, consistent with active burning.

In North Darfur, political and security tensions escalated in late March 2024, with both the SAF and the Rapid Support Forces (RSF) preparing for confrontation in El Fasher by early May. According to the Conflict Observatory, at least 7,800 structures in eastern El Fasher were affected by fighting beginning on May 9, 2024, with NASA FIRMS data indicating widespread fire activity and extensive burning by May 11 (Rothbart et al., 2024a). Earlier, in April 2024, RSF-led forces attacked approximately 17 villages surrounding El Fasher. These attacks caused significant civilian casualties and widespread destruction of residential structures (Sabahelzain et al., 2025). PlanetScope imagery captured active fires in several of these locations on April 13, 2024, including the villages of Jaranga, Muqrin, and Sarafaya (Rothbart et al., 2024b).

Table 1 summarizes the imagery and incident details for all case studies considered in this work. Additionally, Figure 2 illustrates the geographic distribution of the study areas across Sudan. These incidents were selected based on independently reported fire-related damage documented in (Howarth et al., 2024a; Sabahelzain et al., 2025; Howarth et al., 2024b), and manual evaluation and verification conducted by analysts associated with the Sudan Conflict Observatory project.

4. Methodology

4.1. Model architecture

In this study, we adapted and retrained RaVAEn (Růžička et al., 2022), a lightweight convolutional Variational Autoencoder (VAE) framework origi-

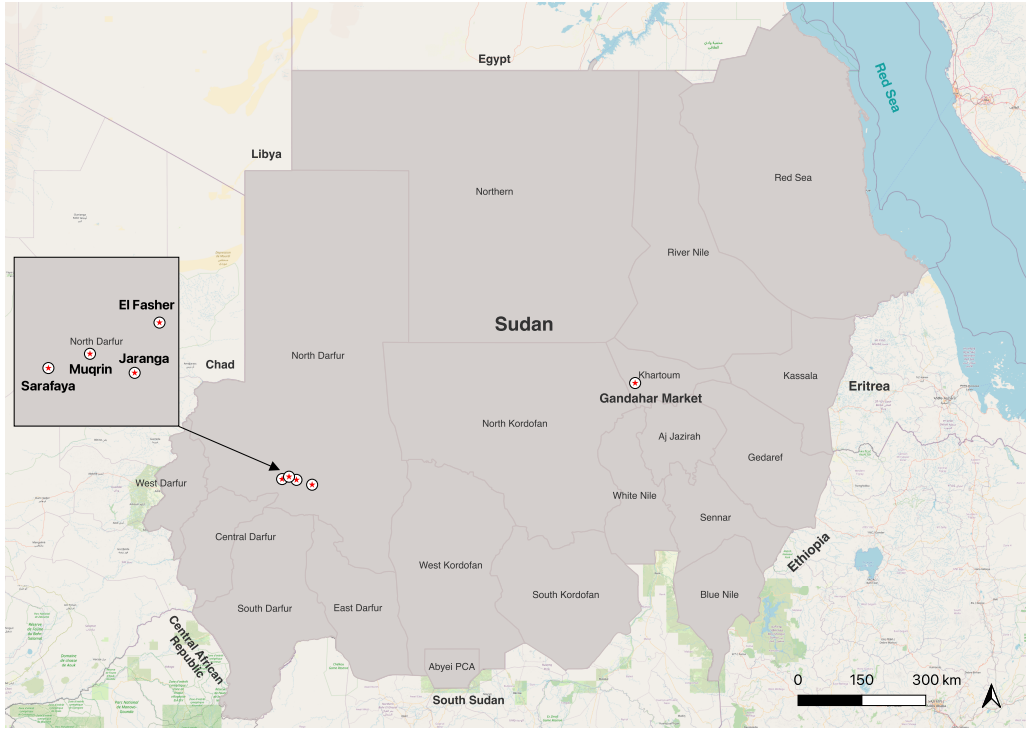


Figure 2: The depiction of study areas used for this research.

nally developed for unsupervised detection of disaster-related surface anomalies across multiple hazard types, including floods, fire burn scars, landslides, and hurricanes. Rather than being tailored to a specific phenomenon, RaVAEn learns a compact latent representation of nominal surface conditions and identifies anomalous patterns as deviations from this learned distribution, making it suitable for detecting previously unseen or irregular events such as conflict-related fires. The original model was designed for 10-band satellite imagery at 10 m spatial resolution. We retrained it for 3 m resolution imagery with four spectral channels (RGB and near-infrared) to better capture fine-scale spatial heterogeneity associated with small, fragmented fire events in urban conflict settings.

The revised model employs a resolution-adaptive Variational Autoencoder (VAE) designed to extract scale-robust surface characteristics from heterogeneous satellite imagery while reducing domain discrepancies across varying ground sampling distances. The model follows an unsupervised encoder-decoder framework composed of four hierarchical stages, with adapta-

tions concentrated in the early layers to address resolution-dependent spatial frequencies present in 10 m and 3 m data. At the input, the encoder applies a frequency decomposition layer, where a fixed Gaussian low-pass filter extracts coarse structural priors and a high-pass residual captures fine-grained texture. These components are concatenated to provide the encoder with explicit access to both coarse structure and fine detail, enabling consistent feature learning across resolutions.

To accommodate scale-variant spatial patterns, standard strided convolutions in the initial stages are replaced with multi-scale convolutional blocks analogous to Atrous Spatial Pyramid structures (Maggiori et al., 2016). These blocks use parallel 3×3 convolutions with increasing dilation rates, fused via a 1×1 convolution. This design enables the encoder to capture multi-scale contextual dependencies and expand its effective receptive field while preserving spatial detail (Chen et al., 2017; Yuan et al., 2018). Anti-aliased downsampling, or BlurPool (Zhang, 2019), implemented as a stride-1 convolution followed by low-pass filtering and pooling, mitigates the loss of high-frequency information and improves shift equivariance when processing higher-resolution imagery. Each downsampling operation is followed by residual convolutional blocks with leaky ReLU activations and normalization layers, while deeper stages retain a conventional residual structure as higher-level semantic features are less sensitive to pixel-level resolution.

The final encoder feature map is aggregated using global pooling and projected onto a 128-dimensional latent space parameterized by a diagonal Gaussian distribution, regularized with a β -VAE objective ($\beta=1$). The decoder mirrors the encoder hierarchy using nearest-neighbor upsampling and convolutional layers, with a linear activation in the output layer. The model is trained end-to-end using the Adam optimizer with a learning rate of 0.001 and a batch size of 128, minimizing a combination of mean squared reconstruction loss and Kullback–Leibler divergence. To improve generalization across spatial resolutions, a scale-augmented training strategy is applied in which imagery is stochastically resampled to simulate continuous transitions in ground sampling distance (Koziarski and Cyganek, 2017). This resampling is applied only during training; inference operates directly on native-resolution imagery, producing resolution-invariant feature embeddings.

While VAEs are commonly used for unsupervised anomaly detection by thresholding reconstruction error for individual inputs (Angerhausen et al., 2022), prior work has shown that reconstruction error can be an unreliable indicator of anomalous behavior in fully unsupervised settings (Merrill and

Eskandarian, 2020). Motivated by these findings, we do not use reconstruction error as the anomaly signal. Instead, the VAE is used as a representation learning framework to embed surface conditions into a compact latent space, in which changes between temporally paired observations can be quantified for change detection.

We trained the model for 200 epochs based on the convergence analysis of the VAE objective on a held-out validation set consisting of 19 scenes. The reconstruction loss decreased rapidly during early training and exhibited diminishing improvements after approximately 80 epochs, while the Kullback–Leibler divergence term stabilized after around 120 epochs, indicating convergence of the latent distribution. Beyond 200 epochs, the total validation loss plateaued and no further gains were observed in downstream change detection performance, suggesting that additional training yielded negligible benefit. Therefore, 200 epochs provide sufficient optimization for stable convergence without incurring unnecessary computational cost.

4.2. Preprocessing and Spectral Alignment

To mitigate sensor-specific radiometric bias and atmospheric variability, we implement a dual-stage normalization pipeline. Initially, to align the 3-meter imagery with the 10-meter reference, we perform Spectral Normalization via Major Axis (MA) Linear Regression Chastain et al. (2019). For each overlapping spectral band b , the calibrated 3-meter reflectance x_{cal} is derived as:

$$x_{\text{cal},b} = \alpha_b \cdot x_{3\text{m},b} + \beta_b \quad (1)$$

where the gain (α) and offset (β) coefficients are empirically derived from near-coincident acquisitions. Following spectral alignment, we address the high dynamic range and non-linear distribution of the near-infrared (NIR) band relative to visible spectra. To ensure balanced feature importance across the multispectral cube, we apply a logarithmic compression followed by robust min-max feature scaling.

Consistent with the original RaVAEn configuration, imagery is partitioned into tiles of 32×32 pixels. Each tile is normalized to the $[-1, +1]$ interval according to:

$$x' = \log(x_{\text{cal}} + \epsilon), \quad x'' = 2 \cdot \frac{x' - P_1(x')}{P_{99}(x') - P_1(x')} - 1 \quad (2)$$

where ϵ is a small constant to ensure numerical stability and P_1, P_{99} represent the 1st and 99th percentiles computed per band across the training distribution. This robust scaling minimizes sensitivity to sensor artifacts and extreme outliers while preserving the variance of surface reflectance characteristics. The resulting transformation parameters are archived and consistently applied during inference to maintain latent space stability.

4.3. Evaluation and Metrics

Training: The model was trained using the WorldFloods dataset (Mateo-Garcia et al., 2021) derived from Sentinel-2 multi-spectral imagery (Fletcher, 2012). The dataset includes four classes of disaster-related surface changes, including fire burn scars. The dataset was selected for its high variance in spectral and textural patterns. Training on diverse disaster-related surface changes encourages the VAE to learn generalized, robust visual primitives rather than overfitting to specific biome characteristics. This capability enables the model to effectively reconstruct nominal arid backgrounds in Sudan and highlight fire-related deviations as anomalies, despite the ecological domain shift. Training was performed on 233 scenes, with a held-out validation set of 19 scenes used to assess convergence and prevent overfitting. Training and validation were conducted on a machine equipped with one NVIDIA H100 GPU, 112 Intel CPU cores, and 2 TB of system memory.

Inference: For conflict monitoring in Sudan, radiometrically calibrated 4-band ortho-analytic imagery with red, green, blue, and near-infrared bands was partitioned into 32×32 pixel tiles. Corresponding pre- and post-incident tiles from the same spatial locations were passed through the encoder to obtain latent embeddings. Anomaly detection is formulated as change detection in latent space rather than reconstruction-based scoring. Anomaly scores were computed using the cosine distance between the latent representations of each tile pair, capturing deviations from nominal surface conditions learned during training. This representation-based comparison reduces sensitivity to absolute radiometric differences and sensor noise, enabling robust detection of fire-affected areas without requiring labeled training data.

Baseline comparison: We implemented a tile-wise cosine distance baseline for comparison. Tiles of size 32×32 pixels were flattened into vectors of raw pixel values across all four bands. Cosine distances between corresponding pre- and post-incident tiles were computed to yield continuous anomaly scores. While spectral indices such as NDVI or BAI could utilize the available visible-NIR bands, they impose fixed arithmetic assumptions about surface

reflectance that vary by biome. We selected the baseline to isolate the benefit of learned latent representations: by holding preprocessing, tile geometry, temporal pairing, and the similarity metric constant, any performance difference reflects the contribution of the VAE encoder, independent of heuristic spectral thresholds, allowing evaluation of whether change detection benefits from representation learning beyond direct pixel-space comparison. Baseline scores were thresholded at the 95th percentile of distances across nominal scenes and aggregated into scene-level prediction maps, enabling direct comparison with VAE-based anomaly scores derived from latent embeddings.

Fire incident labeling: Ground-truth labels were curated as part of the SCO initiative, which analyzes information collected from human rights organizations, ACLED, and field interviews (Etefa, 2026; Rothbart et al., 2024a). Tiles were labeled fire-affected if post-incident imagery revealed burn scars or active fire. Each scene was reviewed by at least three analysts, with discrepancies resolved by consensus, yielding inter-annotator agreement above 90%. To mitigate circularity and spatial uncertainty, fire incidents were further validated using FIRMS and VIIRS datasets and cross-referenced with independent reports (Howarth et al., 2024a,b). Labels were used solely for retrospective evaluation and not for training, threshold optimization, or model selection. Visual interpretation of PlanetScope imagery was restricted specifically to the spatial delineation of burn scars for these pre-verified incidents. This ensures that the model is evaluated on its ability to segment confirmed damage, rather than on incidents defined solely by the imagery itself.

Metrics: Model performance was quantified using the area under the precision–recall curve (AUPRC), which provides a threshold-independent measure of how effectively anomaly scores rank fire-affected tiles above non-fire tiles. AUPRC is preferred over the ROC curve in this setting because fire-affected tiles constitute a small fraction of each scene, and precision–recall analysis provides a more informative evaluation under severe class imbalance. Continuous anomaly scores, derived from cosine distances computed either in the VAE latent embedding space or directly in pixel space for the baseline method, were evaluated against the curated fire labels. Precision and recall were computed by sweeping thresholds across all observed scores to generate binary predictions, producing a precision–recall curve summarizing the trade-off between true and false positives. In addition, representative thresholds were used to report precision, recall, and F1-score for interpretable point estimates. Beyond quantitative metrics, model outputs were also assessed qualitatively by visualizing the spatial distribution of anomalous tiles,

enabling inspection of spatial coherence and localization and illustrating correspondence with observed fire patterns in the imagery.

Near-real-time detection: We define “near-real-time” detection as producing fire anomaly outputs within 24–30 hours of image acquisition. This timeframe includes data acquisition latency (approximately 18–20 hours for PlanetScope imagery), preprocessing and tiling (spectral standardization, log transforms, and 32×32 tile generation in 1–2 hours), and model inference plus postprocessing (reconstruction, scoring, and visualization in 1–2 hours per scene on GPU-enabled hardware). Together, these stages enable rapid situational awareness for monitoring fire-affected areas in conflict settings.

4.4. Imagery details

Planet operates Earth-imaging constellations: PlanetScope (PS), Rapid-Eye (RE), and SkySat (SS). Imagery formats serve various use cases, including deep learning, disaster response, precision agriculture, and temporal image analytics. Planet offers three product lines for PlanetScope imagery: Basic Scene, Ortho Scene, and Ortho Tile. The Basic Scene product is a scaled Top of Atmosphere Radiance (at sensor) and sensor-corrected product, suitable for advanced image processing and geometric correction. Ortho Tiles are multiple orthorectified scenes in a single strip, divided according to a defined grid. Ortho Scenes represent single-frame image captures with post-processing, removing terrain distortions and suitable for cartographic purposes. Ortho Scenes are delivered as visual (RGB) and analytic products (Marta, 2018). In this work, we utilized radiometrically calibrated 4-band ortho-analytic imagery obtained from the PS2 instrument, which captures red, green, blue, and near-infrared channels.

Table 1: Details of satellite imagery used for the study area.

Place	Area (km^2)	Incident date	Before-imagery date	After-imagery date
Gandahar Market	3.072	May 25, 2024	May 13, 2024	May 25, 2024
El Fasher	4.032	May 06-07, 2024	May 02, 2024	May 11, 2024
Muqrin	3.168	Apr 13, 2024	Mar 01, 2024	Apr 13, 2024
Jaranga	1.536	Apr 13, 2024	Mar 01, 2024	Apr 13, 2024
Sarafaya	1.44	Apr 13, 2024	Mar 01, 2024	Apr 13, 2024

4.5. Incident data

The SCO methodology for collecting incident data uses a multi-phase approach combining secondary research and original data collection. Researchers first examine reports from organizations including Human Rights Watch, the World Health Organization, and the United Nations. Additionally, Armed Conflict Location & Event Data (ACLED) catalog is utilized as another complementary source to consolidate the incidents dataset. These sources document civilian targeting and infrastructure destruction, which the SCO then aims to enhance with further analysis or more current accounts from the impacted areas in Sudan. Social media provides direct witness reports and real-time updates for incident verification. By combining these varied streams, the SCO researchers confirm the validity of specific incidents. Furthermore, Sudan Human Rights Hub (SHRH) conducted interviews of individuals on the ground affected by the attacks. Testimony was given only after the research participants received full information about the purpose, scope and use of their information, followed by their consent. Detailed methodology and technical specifications of the incident collection methodology are reported in (Masri et al., 2025)

ACLED catalog compiles and curates a dataset of individual political disorder events across the world. Its focus is on political violence and protest, and it monitors the activity of a variety of conflict actors and armed groups, as well as multiple forms of unrest. Unlike other datasets that use machine-led coding, ACLED relies on a researcher-led data collection process that allows for the incorporation of conflict and protest events from a wide range of sources, including local-language media, conflict observatories and other situation reports, which mitigates over-reliance on international news agencies (Carboni and Raleigh, 2024)

Since the scope of the SCO reporting is broader, ranging from infrastructure damages to civil rights violations to gender violence, we manually selected the incidents identified as destruction attributed to fires in the conflict. The rationale for selecting such incidents was that satellite imagery can capture and validate the visual signatures of fire-related destruction reported by the SCO.

5. Results

We evaluate the effectiveness of the proposed deep learning-based fire detection approach by comparing model outputs against a baseline that

computes cosine distance between pre- and post-incident image tiles after identical preprocessing. Performance was assessed across five case studies in Sudan using qualitative visual inspection of prediction maps and quantitative metrics. To quantify uncertainty and robustness, we computed 95% confidence intervals for all metrics via 1,000 bootstrap resamples of tiles within each scene. Additionally, paired Wilcoxon signed-rank tests were applied to AUPRC values obtained from identical bootstrap resamples of tiles for the baseline and proposed method, ensuring matched, nonparametric comparison under identical sampling conditions. In addition to absolute performance metrics, we report Cohen's d to quantify the magnitude of improvement of the proposed VAE-based approach relative to the baseline. Figures 3 and 4 present visual comparisons for Jaranga and El Fasher, respectively.

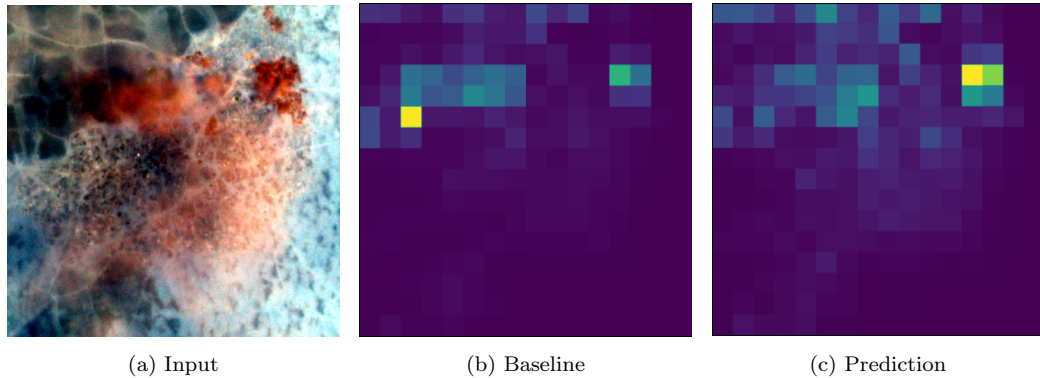


Figure 3: Comparison of baseline with prediction in Jaranga.

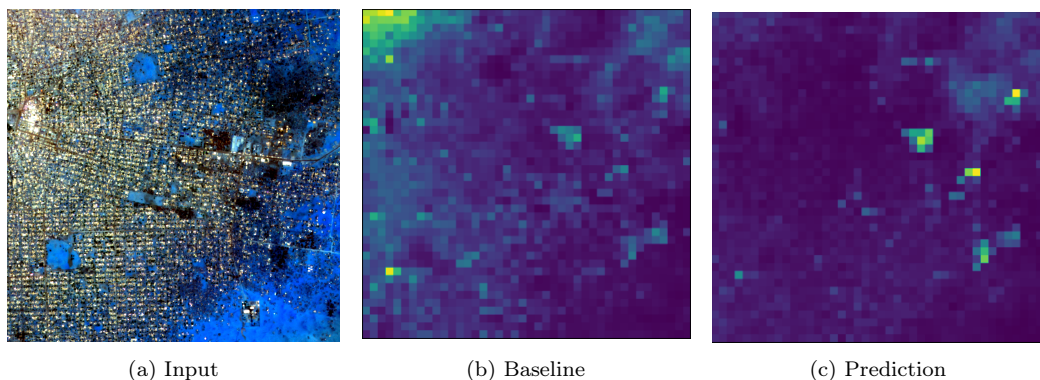


Figure 4: Comparison of baseline with prediction in El Fasher.

Results indicate that the baseline method tends to replicate fine-grained details from the input imagery and is highly sensitive to noise, misregistration, and small radiometric or geometric variations. In contrast, the proposed approach captures higher-level latent features, facilitating more robust delineation of fire-affected areas from background changes.

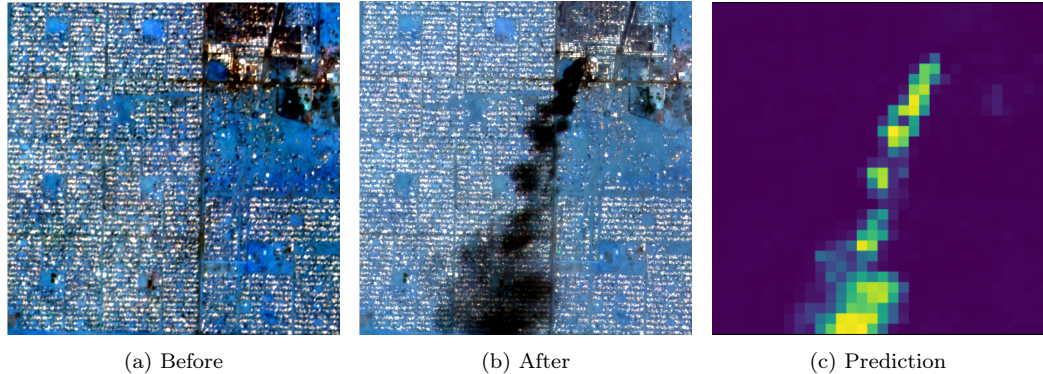


Figure 5: Comparison of before and after input imagery with an active fire prediction in Gandahar Market with a smoke plume.

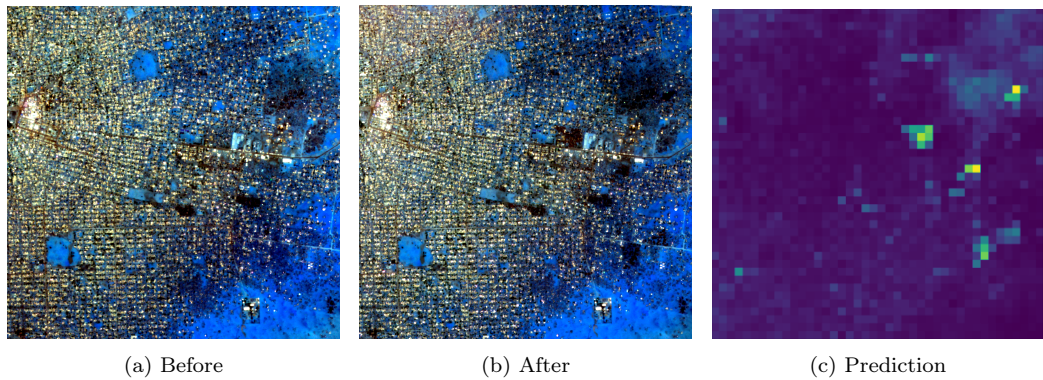


Figure 6: Comparison of before and after input imagery to detect burn scars after occurrence of fire incidents in El Fasher with multiple charred places.

Figures 5 to 9 provide qualitative results across all study areas. The model successfully detects active fires and associated smoke plumes in Gandahar Market in Figure 5. Similarly, Figure 6 demonstrates the model’s ability to identify burn scars following fire incidents. We note that large areas of El Fasher are burned after multiple successive fire incidents, leaving extensive

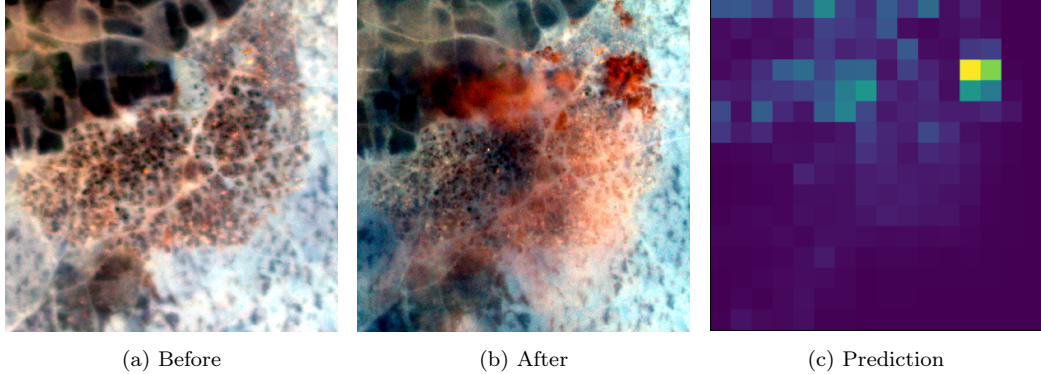


Figure 7: Comparison of before and after input imagery with an active fire prediction in Jaranga.

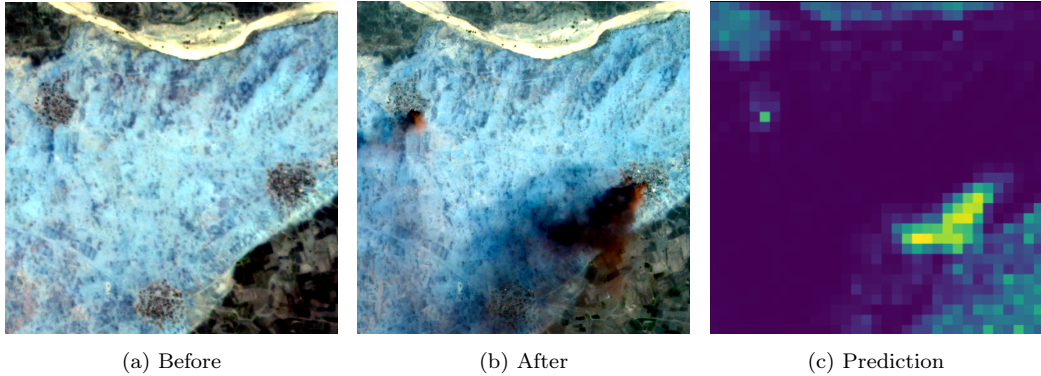


Figure 8: Comparison of before and after input imagery with multiple closely spaced active fires in Muqrin.

swaths of charred surfaces. Even in relatively complex images, the model performs well in delineating severely burned areas. Figure 7 shows that multiple simultaneous fires are detected in Jaranga, while previously impacted locations are correctly identified in Muqrin (Figure 8). Finally, Figure 9 illustrates accurate delineation of recently burned surfaces in Sarafaya. Across all cases, predicted fire-affected regions exhibit strong spatial coherence and align well with independently verified ground-truth labels.

5.1. Quantitative Performance

Tables 2–6 summarize bootstrapped metrics for each location and imagery configuration. Across all sites, the proposed VAE-based approach consistently outperformed the baseline. Median relative AUPRC improvements

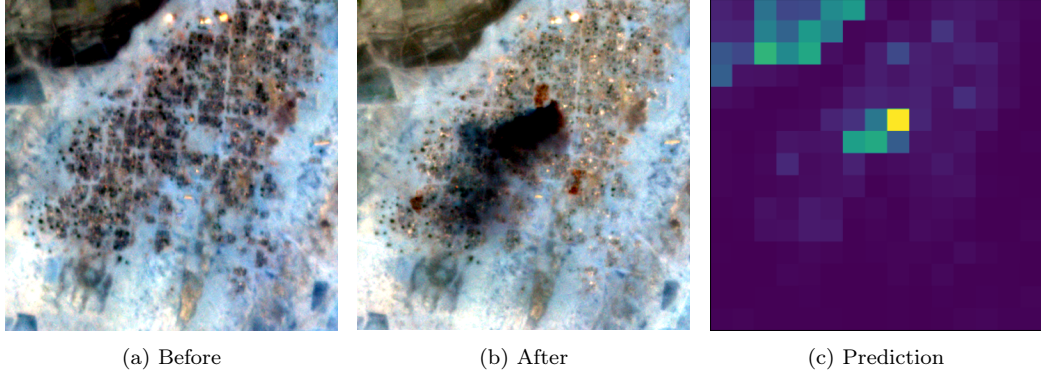


Figure 9: Comparison of before and after input imagery with an impact of fires in Sarafaya.

ranged from 18% to 40%, corresponding to moderate-to-large effect sizes (Cohen’s $d = 0.8\text{--}1.5$). Relative improvement is computed using median values as $(\text{AUPRC}_{\text{pred}} - \text{AUPRC}_{\text{base}})/\text{AUPRC}_{\text{base}}$. Paired statistical tests confirmed that differences were statistically significant ($p < 0.01$) for all locations. Improvements are particularly pronounced in complex urban and peri-urban settings such as El Fasher and Jaranga, where fires are spatially fragmented and embedded in heterogeneous backgrounds. In Muqrin and Sarafaya, which exhibit clearer fire signatures, the model achieves AUPRC values exceeding 0.9. We note that the confidence interval widths vary modestly across sites due to differences in tile counts and spatial heterogeneity, but remain narrow owing to the large number of tiles per scene.

5.2. Observations on False Positives and False Negatives

Analysis of tile-level outputs revealed patterns in prediction errors. False positives were most commonly associated with residual burned material from prior incidents or structural debris resembling charred surfaces, reflecting the model’s sensitivity to broader damage signatures. False negatives occurred primarily for small, fragmented fires below the 3 m sensor resolution in densely built urban areas. These error modes are consistent with known limitations of optical imagery in conflict environments and are considered acceptable within operational settings that prioritize rapid situational awareness over exhaustive error minimization (Zwijnenburg and Ballinger, 2023). Despite these challenges, recall remained relatively high, consistent with the near-real-time monitoring objective that prioritizes high-sensitivity detection of fire-affected areas.

Table 2: Gandahar Market: Bootstrapped metrics (median and 95% CI) and Cohen’s d .

Imagery	Metric	Baseline	Prediction	Cohen’s d
4-band	AUPRC	0.584 (0.562–0.605)	0.747 (0.729–0.765)	1.12
	Precision	0.63 (0.61–0.65)	0.71 (0.69–0.73)	0.87
	Recall	0.55 (0.53–0.57)	0.74 (0.72–0.76)	1.33
	F1	0.59 (0.57–0.61)	0.72 (0.70–0.74)	1.06
8-band	AUPRC	0.619 (0.597–0.640)	0.825 (0.807–0.841)	1.38
	Precision	0.66 (0.64–0.68)	0.76 (0.74–0.78)	0.96
	Recall	0.57 (0.55–0.59)	0.77 (0.75–0.79)	1.40
	F1	0.61 (0.59–0.63)	0.76 (0.74–0.78)	1.20
Time series	AUPRC	0.599 (0.578–0.618)	0.794 (0.775–0.811)	1.24
	Precision	0.64 (0.62–0.66)	0.73 (0.71–0.75)	0.89
	Recall	0.56 (0.54–0.58)	0.75 (0.73–0.77)	1.35
	F1	0.59 (0.57–0.61)	0.74 (0.72–0.76)	1.13

Table 3: El Fasher: Bootstrapped metrics (median and 95% CI) and Cohen’s d .

Imagery	Metric	Baseline	Prediction	Cohen’s d
4-band	AUPRC	0.447 (0.430–0.464)	0.695 (0.678–0.710)	1.45
	Precision	0.52 (0.50–0.54)	0.63 (0.61–0.65)	0.88
	Recall	0.48 (0.46–0.50)	0.70 (0.68–0.72)	1.35
	F1	0.50 (0.48–0.52)	0.66 (0.64–0.68)	1.15
8-band	AUPRC	0.346 (0.331–0.360)	0.471 (0.455–0.486)	0.90
	Precision	0.44 (0.42–0.46)	0.53 (0.51–0.55)	0.72
	Recall	0.38 (0.36–0.40)	0.48 (0.46–0.50)	0.81
	F1	0.41 (0.39–0.43)	0.50 (0.48–0.52)	0.78
Time series	AUPRC	0.407 (0.392–0.422)	0.646 (0.630–0.662)	1.32
	Precision	0.49 (0.47–0.51)	0.61 (0.59–0.63)	0.86
	Recall	0.43 (0.41–0.45)	0.65 (0.63–0.67)	1.22
	F1	0.45 (0.43–0.47)	0.63 (0.61–0.65)	1.05

Table 4: Muqrin: Bootstrapped metrics (median and 95% CI) and Cohen’s d .

Imagery	Metric	Baseline	Prediction	Cohen’s d
4-band	AUPRC	0.673 (0.655–0.690)	0.929 (0.915–0.941)	1.54
	Precision	0.71 (0.69–0.73)	0.90 (0.88–0.92)	1.12
	Recall	0.63 (0.61–0.65)	0.94 (0.92–0.95)	1.68
	F1	0.67 (0.65–0.69)	0.92 (0.90–0.94)	1.44
8-band	AUPRC	0.691 (0.673–0.708)	0.935 (0.921–0.946)	1.48
	Precision	0.73 (0.71–0.75)	0.91 (0.89–0.93)	1.09
	Recall	0.65 (0.63–0.67)	0.94 (0.92–0.95)	1.61
	F1	0.68 (0.66–0.70)	0.93 (0.91–0.94)	1.41
Time series	AUPRC	0.683 (0.665–0.700)	0.938 (0.924–0.950)	1.52
	Precision	0.72 (0.70–0.74)	0.92 (0.90–0.94)	1.16
	Recall	0.64 (0.62–0.66)	0.95 (0.93–0.96)	1.64
	F1	0.68 (0.66–0.70)	0.93 (0.91–0.95)	1.44

Table 5: Jaranga: Bootstrapped metrics (median and 95% CI) and Cohen’s d .

Imagery	Metric	Baseline	Prediction	Cohen’s d
4-band	AUPRC	0.417 (0.401–0.433)	0.630 (0.612–0.646)	1.21
	Precision	0.50 (0.48–0.52)	0.61 (0.59–0.63)	0.87
	Recall	0.43 (0.41–0.45)	0.66 (0.64–0.68)	1.33
	F1	0.46 (0.44–0.48)	0.63 (0.61–0.65)	1.12
8-band	AUPRC	0.513 (0.495–0.531)	0.722 (0.703–0.738)	1.15
	Precision	0.56 (0.54–0.58)	0.68 (0.66–0.70)	0.91
	Recall	0.49 (0.47–0.51)	0.70 (0.68–0.72)	1.22
	F1	0.52 (0.50–0.54)	0.69 (0.67–0.71)	1.09
Time series	AUPRC	0.474 (0.457–0.491)	0.671 (0.652–0.688)	1.18
	Precision	0.53 (0.51–0.55)	0.65 (0.63–0.67)	0.89
	Recall	0.46 (0.44–0.48)	0.68 (0.66–0.70)	1.26
	F1	0.49 (0.47–0.51)	0.66 (0.64–0.68)	1.12

Table 6: Sarafaya: Bootstrapped metrics (median and 95% CI) and Cohen’s d .

Imagery	Metric	Baseline	Prediction	Cohen’s d
4-band	AUPRC	0.686 (0.668–0.704)	0.918 (0.905–0.932)	1.50
	Precision	0.73 (0.71–0.75)	0.91 (0.89–0.93)	1.10
	Recall	0.66 (0.64–0.68)	0.94 (0.92–0.95)	1.62
	F1	0.69 (0.67–0.71)	0.92 (0.90–0.94)	1.42
8-band	AUPRC	0.676 (0.658–0.693)	0.926 (0.913–0.939)	1.55
	Precision	0.72 (0.70–0.74)	0.92 (0.90–0.94)	1.19
	Recall	0.67 (0.65–0.69)	0.95 (0.93–0.96)	1.64
	F1	0.69 (0.67–0.71)	0.93 (0.91–0.95)	1.45
Time series	AUPRC	0.694 (0.676–0.711)	0.929 (0.915–0.942)	1.52
	Precision	0.74 (0.72–0.76)	0.92 (0.90–0.94)	1.12
	Recall	0.67 (0.65–0.69)	0.95 (0.93–0.96)	1.61
	F1	0.70 (0.68–0.72)	0.93 (0.91–0.95)	1.42

5.3. Sufficiency of 4-band Imagery

Across all locations, 4-band PlanetScope imagery captured most discriminative features for fire detection. While modest improvements were observed with 8-band imagery or short temporal sequences (median relative AUPRC gains of 3–7% across tested scenes), statistical testing indicated that these improvements were small and often not operationally significant. We note that this observation is specific to the scenes and fire types analyzed; additional spectral bands may improve performance in areas with more subtle spectral signatures of fire or more heterogeneous land cover. In El Fasher, the modest improvement observed with 8-band imagery, and the degraded baseline performance, are likely due to increased sensitivity to inter-band noise and residual misregistration in a highly heterogeneous urban setting.

5.4. Summary

Overall, the proposed VAE-based approach demonstrates robust and statistically significant improvements over a pixel-space baseline. Bootstrapped confidence intervals confirm stability across scenes, effect sizes indicate substantial performance gains, and observed error patterns provide actionable insight for operational near-real-time monitoring of conflict-related fires.

All experiments are compatible with the near-real-time processing pipeline described in Section 4.3, producing outputs within 24–30 hours of image

acquisition. Consistent with prior work (Růžička et al., 2022), these results demonstrate that latent representation-based change detection substantially outperforms direct pixel-space comparisons. Considering the acquisition, preprocessing, and computational overheads of multi-spectral and multi-temporal inputs, the limited performance gains observed with additional data modalities indicate that the proposed lightweight 4-band configuration offers a favorable trade-off between accuracy and operational efficiency for near-real-time conflict monitoring. We note that all quantitative results are conditioned on the availability of cloud-free optical imagery and accurate co-registration between pre- and post-incident scenes.

6. Discussion

Our findings demonstrate that near-real-time detection of conflict-related fire damage is feasible using near-daily PlanetScope imagery combined with latent representation-based change detection. Across multiple case studies, the proposed VAE-based approach outperformed a pixel-space cosine distance baseline, producing spatially coherent outputs suitable for rapid situational awareness. These findings align with prior research demonstrating the potential of latent representation learning in satellite-based change detection (Bennett et al., 2022). Additionally, results indicate that 4-band imagery captures most of the discriminative information required for fire detection, with additional spectral bands or short temporal sequences providing only modest gains. Compared with public satellites such as MODIS, VIIRS, and Sentinel-2, PlanetScope provides a practical balance of spatial resolution, revisit frequency, and accessibility. However, its limited 4–8 band coverage constrains detection of subtle spectral signatures compared with Sentinel-2’s 13 bands. This trade-off reflects methodological choices common in conflict monitoring: 3 m resolution commercial imagery allows near-daily monitoring at manageable cost, while very high-resolution imagery remains limited due to availability and expense (Bennett et al., 2022). This work highlights the importance of interdisciplinary integration. Verification of detected incidents, uncertainty quantification, and operational relevance require input from peace and conflict research, humanitarian studies, and remote sensing expertise. Prior work emphasizes that automated satellite detection alone does not produce actionable insight; coordinated approaches are needed to interpret results, ensure reliability, and support evidence-based decision-making in conflict-affected contexts (Ghioni et al., 2024; Duursma,

2023).

7. Conclusion

A civil war in Sudan, primarily between the Sudan Armed Forces (SAF) and the Rapid Support Forces (RSF), has caused widespread civilian casualties and displacement (Ahmed et al., 2025), with over 1,400 violent incidents targeting civilians, resulting in 61,000 war-related deaths and 12 million displaced people (Rothbart et al., 2025). This study demonstrates that conflict-related fire damage in Sudan can be detected in near-real-time using PlanetScope imagery and latent representation-based change detection. The VAE-based approach reliably detected fire damage, with 4-band imagery providing the most relevant information and additional bands or short temporal sequences offering only minor improvements. The study contributes an operationally focused integration of remote sensing, machine learning, and conflict analysis to support humanitarian assessment in data-scarce regions. We note some limitations of the work: it is based on a small number of case studies in Sudan, which limits generalizability, the baseline comparison relies on a simple cosine distance method, and dependence on commercial PlanetScope imagery introduces constraints on data access, cost, and reproducibility. Despite these limitations, the results demonstrate the potential of lightweight, latent representation-based methods for near-real-time monitoring of conflict-related fire damage, illustrating a practical trade-off between accuracy, data availability, and operational efficiency for rapid conflict monitoring when higher-resolution or ground-based data are unavailable.

Acknowledgements

The researchers involved in the SCO project include the authors of this article as well as the following analysts: Moneim Adam, Mathieu Bere, Hind Fadul, Anusha Sriranganathanmalarvizhi, Zifu Wang, David Wong and Chaowei Yang.

This project was supported by computing resources provided by the Office of Research Computing at George Mason University (URL: <https://orc.gmu.edu>) and funded in part by grants from the National Science Foundation (Awards Number 1625039, 2018631, and 2109647).

Funding

The research conducted in this article was funded by the United States Department of State and contracted by The MITRE Corporation.

Conflicts of Interest

The authors declare no conflicts of interest.

Data availability

The data that support the findings of this study are available upon a reasonable request from the corresponding author. The data are not publicly available due to privacy or licensing restrictions.

Code availability

The code is available in a GitHub repository at https://github.com/heykuldip/nrt_conflict_monitoring

References

Abubakr, B., Gjeloshi, B., Pfoser, D., Rothbart, D., 2024. Sudan war: Retrospective on health care system destruction.

Ahmed, O.S., Eltahir, M.E., Abdelkareem, A.N.Y., Al-Rawashdeh, A.Z., Ahmed, A.S., 2025. Is calling the saf-rsf conflict a ‘dirty war’ an objective description or a moral judgment? a critical analysis of the ongoing war in sudan (2023–present). *Cogent Social Sciences* 11, 2586199.

de Almeida Pereira, G.H., Fusioka, A.M., Nassu, B.T., Minetto, R., 2021. Active fire detection in landsat-8 imagery: A large-scale dataset and a deep-learning study. *ISPRS Journal of Photogrammetry and Remote Sensing* 178, 171–186.

Alrawa, S.S., Alfadul, E.S., Elhassan, M.M.A., Hammad, N., 2023. Five months into conflict: near total collapse of cancer services in sudan. *ecancermedicalscience* 17, ed128.

An, J., Cho, S., 2015. Variational autoencoder based anomaly detection using reconstruction probability. Special lecture on IE 2, 1–18.

Angerhausen, D., Bickel, V.T., Adam, L., 2022. Unsupervised distribution learning for lunar surface technosignature detection. *Authorea Preprints* .

Aung, T.S., Overland, I., Vakulchuk, R., Xie, Y., 2021. Using satellite data and machine learning to study conflict-induced environmental and socioeconomic destruction in data-poor conflict areas: The case of the rakhine conflict. *Environmental Research Communications* 3, 025005.

Avtar, R., Kouuser, A., Kumar, A., Singh, D., Misra, P., Gupta, A., Yunus, A.P., Kumar, P., Johnson, B.A., Dasgupta, R., et al., 2021. Remote sensing for international peace and security: Its role and implications. *Remote Sensing* 13, 439.

Bazi, Y., Bashmal, L., Rahhal, M.M.A., Dayil, R.A., Ajlan, N.A., 2021. Vision transformers for remote sensing image classification. *Remote Sensing* 13, 516.

Bennett, M., Van Den Hoek, J., Zhao, B., Prishchepov, A., 2022. Improving satellite monitoring of armed conflicts. *Earth's Future* 10, e2022EF002904.

Bergamasco, L., Saha, S., Bovolo, F., Bruzzone, L., 2022. Unsupervised change detection using convolutional-autoencoder multiresolution features. *IEEE Transactions on Geoscience and Remote Sensing* 60, 1–19.

Birch, I., Carter, B., Satti, H.A., 2024. Effective social protection in conflict: Findings from Sudan. Technical Report. The Institute of Development Studies and Partner Organisations. URL: <https://hdl.handle.net/20.500.12413/18235>.

Boroujeni, S.P.H., Razi, A., Khoshdel, S., Afghah, F., Coen, J.L., O'Neill, L., Fule, P., Watts, A., Kokolakis, N.M.T., Vamvoudakis, K.G., 2024. A comprehensive survey of research towards ai-enabled unmanned aerial systems in pre-, active-, and post-wildfire management. *Information Fusion* , 102369.

Braun, A., 2018. Assessment of building damage in raqqa during the syrian civil war using time-series of radar satellite imagery. *GI_Forum 2018*, 6, 228–242.

Bromley, L., 2010. Relating violence to modis fire detections in darfur, sudan. *International Journal of Remote Sensing* 31, 2277–2292.

Carboni, A., Raleigh, C., 2024. Collecting conflict data worldwide: Acled's contribution, in: Open Source Investigations in the Age of Google. World Scientific, pp. 171–187.

Chastain, R., Housman, I., Goldstein, J., Finco, M., Tenneson, K., 2019. Empirical cross sensor comparison of sentinel-2a and 2b msi, landsat-8 oli, and landsat-7 etm+ top of atmosphere spectral characteristics over the conterminous united states. *Remote sensing of environment* 221, 274–285.

Chen, L.C., Papandreou, G., Schroff, F., Adam, H., 2017. Rethinking atrous convolution for semantic image segmentation. *arXiv preprint arXiv:1706.05587* .

Cornebise, J., Worrall, D., Farfour, M., Marin, M., 2018. Witnessing atrocities: quantifying villages destruction in darfur with crowdsourcing and transfer learning, in: Proc. AI for Social Good NeurIPS2018 Workshop, NeurIPS'18.

Dahab, M., AbuKoura, R., Checchi, F., Ahmed, A., Abdalla, O., Ibrahim, M., Abdelmagid, N., Alabden, I.Z., Omer, L., Alhaffar, M., et al., 2025. War-time mortality in sudan: a multiple systems estimation analysis. *The Lancet Global Health* 13, e1583–e1590.

Di Martino, T., Le Saux, B., Guinvarc'h, R., Thirion-Lefevre, L., Colin, E., 2023. Detection of forest fires through deep unsupervised learning modeling of sentinel-1 time series. *ISPRS International Journal of Geo-Information* 12, 332.

Duursma, A., 2023. Peacekeeping, mediation, and the conclusion of local ceasefires in non-state conflicts. *Journal of Conflict Resolution* 67, 1405–1429.

Eljack, M.M.F., Elhadi, Y.A.M., Mahgoub, E.A.A., Ahmed, K.A.H.M., Mohamed, M.T.A.A., Elnaiem, W., Mohamedsharif, A., Nour, A.B., Muhammed, A.E.M., Gebril, M.S.M., et al., 2023. Physician experiences with teleconsultations amidst conflict in sudan. *Scientific Reports* 13, 22688.

Etefa, T., 2026. The fall of khartoum: Understanding the war in sudan. *The Journal of Oromo Studies* 30.

Fletcher, K., 2012. SENTINEL 2: ESA's Optical High-Resolution Mission for GMES Operational Services. European Space Agency.

Franquesa, M., Stehman, S.V., Chuvieco, E., 2022. Assessment and characterization of sources of error impacting the accuracy of global burned area products. *Remote Sensing of Environment* 280, 113214.

Ghioni, R., Taddeo, M., Floridi, L., 2024. Open source intelligence and ai: a systematic review of the gelsi literature. *AI & society* 39, 1827–1842.

Hally, B., Wallace, L., Reinke, K., Jones, S., Skidmore, A., 2019. Advances in active fire detection using a multi-temporal method for next-generation geostationary satellite data. *International journal of digital earth* 12, 1030–1045.

Hassan, I.N., Ahmed, S., 2025. Gender-based violence and displacement in darfur's war. *The Lancet* 406, 2919–2920.

Howarth, C.N., Khoshnood, K., Raymond, N.A.e.a., 2024a. Confirmation of nine arson attacks west of el-fasher, sudan.

Howarth, C.N., Khoshnood, K., Raymond, N.A.e.a., 2024b. Confirmation of sudan armed forces bombardment consistent with rapid support forces present in el-fasher.

Jenerowicz, M., Kemper, T., Pesaresi, M., Soille, P., et al., 2010. Post-event damage assessment using morphological methodology on 0.5 m resolution satellite data. *Italian Journal of Remote Sensing* 42, 37–47.

Kahraman, F., Imamoglu, M., Ates, H.F., 2016. Battle damage assessment based on self-similarity and contextual modeling of buildings in dense urban areas, in: 2016 IEEE International Geoscience and Remote Sensing Symposium (IGARSS), IEEE. pp. 5161–5164.

Kingma, D.P., Welling, M., et al., 2013. Auto-encoding variational bayes.

Koziarski, M., Cyganek, B., 2017. Image recognition with deep neural networks in presence of noise—dealing with and taking advantage of distortions. *Integrated Computer-Aided Engineering* 24, 337–349.

Kurnaz, B., Bayik, C., Abdikan, S., 2020. Forest fire area detection by using landsat-8 and sentinel-2 satellite images: A case study in mugla, turkey. Preprint at Research Square URL: <https://doi.org/10.21203/rs.3.rs-26787/v1>.

Lee, J., Xu, J.Z., Sohn, K., Lu, W., Berthelot, D., Gur, I., Khaitan, P., Koupparis, K., Kowatsch, B., et al., 2020. Assessing post-disaster damage from satellite imagery using semi-supervised learning techniques. arXiv preprint arXiv:2011.14004 .

Maggiori, E., Tarabalka, Y., Charpiat, G., Alliez, P., 2016. Convolutional neural networks for large-scale remote-sensing image classification. *IEEE Transactions on geoscience and remote sensing* 55, 645–657.

Marta, S., 2018. Planet imagery product specifications. Planet Labs: San Francisco, CA, USA 91, 170.

Marx, A., Windisch, R., Kim, J.S., 2019. Detecting village burnings with high-cadence smallsats: A case-study in the rakhine state of myanmar. *Remote Sensing Applications: Society and Environment* 14, 119–125.

Masri, Y., Malarvizhi, A.S., Ahmed, S., Stover, T., Wang, Z., Rothbart, D., Bere, M., Wong, D., Pfoser, D., Yang, C., 2025. Automating data collection to support conflict analysis: Scraping the internet for monitoring hourly conflict in sudan. *Cloud Computing and Data Science* .

Mateo-Garcia, G., Veitch-Michaelis, J., Smith, L., Oprea, S.V., Schumann, G., Gal, Y., Baydin, A.G., Backes, D., 2021. Towards global flood mapping onboard low cost satellites with machine learning. *Scientific reports* 11, 7249.

Merrill, N., Eskandarian, A., 2020. Modified autoencoder training and scoring for robust unsupervised anomaly detection in deep learning. *IEEE Access* 8, 101824–101833.

Milton, S., Antaby, M., Dellai, H., Idrees, A., 2025. Counting the costs of war: A holistic, multi-level assessment of the impact of conflict on sudan. *African Security Review* , 1–17.

Mueller, H., Groeger, A., Hersh, J., Matranga, A., Serrat, J., 2021. Monitoring war destruction from space using machine learning. *Proceedings of the national academy of sciences* 118, e2025400118.

Narvaez Luces, O.D.R., Pham, M.T., Poterek, Q., Braun, R., 2023. Burnt area extraction from high-resolution satellite images based on anomaly detection, in: *Joint European Conference on Machine Learning and Knowledge Discovery in Databases*, Springer. pp. 448–457.

Pleniou, M., Koutsias, N., 2025. The role of spectral vs spatial resolution of satellite data on the accuracy of mapping unburned vegetation within fire scar perimeters. *Science of Remote Sensing* , 100241.

Racek, D., Zhang, Q., Thurner, P.W., Zhu, X.X., Kauermann, G., 2025. Unsupervised detection of building destruction during war from publicly available radar satellite imagery. *PNAS nexus* 4, pgaf367.

Rothbart, D., Abubakr, B., Adam, M., Bere, M., Fadul, H., Gjeloshi, B., Lynch, J., Pfoser, D., Singh Atwal, K., Sriranganathanmalarvizhi, A., Wang, Z., Wong, D., Yang, C., 2024a. Impact on civilians from fighting in el fasher, north darfur, may 9 - 27 2024.

Rothbart, D., Abubakr, B., Adam, M., Bere, M., Fadul, H., Gjeloshi, B., Lynch, J., Pfoser, D., Singh Atwal, K., Sriranganathanmalarvizhi, A., Wang, Z., Wong, D., Yang, C., 2024b. Military clashes in north darfur, april 6-18 2024.

Rothbart, D., Abubakr, B., Gjeloshi, B., Pfoser, D., 2025. Sudan at war with itself: Civilian devastation in the civil war. *Conflict Resolution Quarterly*

Růžička, V., Vaughan, A., De Martini, D., Fulton, J., Salvatelli, V., Bridges, C., Mateo-Garcia, G., Zantedeschi, V., 2022. Ravæn: unsupervised change detection of extreme events using ml on-board satellites. *Scientific reports* 12, 16939.

Sabahelzain, M.M., Mohieldin, A., Awadalla, H., 2025. El fasher crisis: over 500 days under siege amid global inaction. *The Lancet* 406, 2417–2418.

Saleh, A., Zulkifley, M.A., Harun, H.H., Gaudreault, F., Davison, I., Spraggon, M., 2024. Forest fire surveillance systems: A review of deep learning methods. *Heliyon* 10.

Schroeder, W., Oliva, P., Giglio, L., Quayle, B., Lorenz, E., Morelli, F., 2016. Active fire detection using landsat-8/oli data. *Remote sensing of environment* 185, 210–220.

Seydi, S.T., Saeidi, V., Kalantar, B., Ueda, N., Halin, A.A., 2022. Firenet: A deep learning framework for active forest fire detection. *Journal of Sensors* 2022, 8044390.

Sticher, V., Wegner, J.D., Pfeifle, B., 2023. Toward the remote monitoring of armed conflicts. *PNAS nexus* 2, pgad181.

Toan, N.T., Cong, P.T., Hung, N.Q.V., Jo, J., 2019. A deep learning approach for early wildfire detection from hyperspectral satellite images, in: 2019 7th International Conference on Robot Intelligence Technology and Applications (RiTA), IEEE. pp. 38–45.

Xu, Y., Zhang, L., Du, B., Zhang, L., 2022. Hyperspectral anomaly detection based on machine learning: An overview. *IEEE Journal of Selected Topics in Applied Earth Observations and Remote Sensing* 15, 3351–3364.

Yuan, Q., Wei, Y., Meng, X., Shen, H., Zhang, L., 2018. A multiscale and multidepth convolutional neural network for remote sensing imagery pan-sharpening. *IEEE Journal of Selected Topics in Applied Earth Observations and Remote Sensing* 11, 978–989.

Zhang, R., 2019. Making convolutional networks shift-invariant again, in: International conference on machine learning, PMLR. pp. 7324–7334.

Zhao, Y., Ban, Y., Sullivan, J., 2023. Tokenized time-series in satellite image segmentation with transformer network for active fire detection. *IEEE Transactions on Geoscience and Remote Sensing* 61, 1–13.

Zwijnenburg, W., Ballinger, O., 2023. Leveraging emerging technologies to enable environmental monitoring and accountability in conflict zones. *International Review of the Red Cross* 105, 1497–1521.